



Origin and Petrogenetic Implications of Spessartine Garnet in Highly-Fractionated Granite from the Central Eastern Desert of Egypt

Mabrouk SAMI^{1,2,*}, Theodoros NTAFLS², Haroun A. MOHAMED¹, Esam S. FARAHAT¹, Christoph HAUZENBERGER³, Nasser M. MAHDY⁴, Khaled M. ABDEL FADIL⁵ and Douaa FATHY¹

¹ *Geology Department, Faculty of Science, Minia University, El-Minia 61519, Egypt*

² *Department of Lithospheric Research, University of Vienna, Althanstrasse 14, A-1090 Vienna, Austria*

³ *Institute of Mineralogy and Petrology, Karl-Franzens University, Graz, Austria*

⁴ *Nuclear Materials Authority, P.O. 530, El-Maadi, Cairo, Egypt*

⁵ *Geology Department, Faculty of Science, Sohag University, Egypt*

Abstract: A highly-fractionated garnet-bearing muscovite granite represents the marginal granitic facies of the Abu-Diab multiphase pluton in the Central Eastern Desert of Egypt. New electron microprobe analyses (EMPA) and laser ablation inductively coupled plasma mass spectrometry (LA-ICP-MS) data from garnets are reported, in order to constrain their origin and genesis. Garnet in the Abu-Diab host granite is euhedral to subhedral, generally homogeneous and, in rare cases, it shows weak zonation. The garnet contains appreciable amounts of MnO and FeO, with lesser amounts of MgO and CaO, yielding an end-member formula of $\text{Sps}_{61-72}\text{Alm}_{25-35}\text{Prp}_{1-4}\text{Adr}_{0-1}$. Moreover, it is depleted in large ion lithophile elements (LILE) with lower values of Ba, Nb and Sr relative to the primitive mantle. Additionally, it contains high concentrations of HREE and Y and their REE pattern shows strong negative Eu anomalies. The garnet was crystallized under relatively low temperature (646°C–591°C) and pressure (< 3 kbar) conditions. The textural and chemical features indicate that the garnet is magmatic in origin and is chemically similar to that from highly-fractionated A-type granite. It was probably formed at the expense of biotite in a highly-evolved MnO-rich magma and/or by hydroxyl complexing of Mn during the ascending fluid phases.

Key words: spessartine garnet, LA-ICP-MS, A-type granite, Abu-Diab, Egypt

Citation: Sami et al., 2020. Origin and Petrogenetic Implications of Spessartine Garnet in Highly-Fractionated Granite from the Central Eastern Desert of Egypt. *Acta Geologica Sinica (English Edition)*, 94(3): 763–776. DOI: 10.1111/1755-6724.13883

1 Introduction

Garnet, with various compositions, occurs as an accessory mineral and crystallizes under certain petrogenetic conditions in different granitic rock types. The abundant occurrence of magmatic garnet has been reported in pegmatites, aplite dikes and peraluminous S-type granites (Dahlquist et al. 2007; Müller et al. 2012). A small occurrence of magmatic garnet members has been recorded in I- and A-type ($\text{SiO}_2 \geq 70\%$) peraluminous granites (du Bray, 1988; Miller and Stoddard, 1981; Wu et al. 2004; Zhang et al. 2012). Garnet is an important geochemical tracer due to its ability to fractionate HREE from LREE (Gaspar et al., 2008). Garnet can also give insights into granitic magma sources and its origin has recently drawn the attention of many workers (Gharib, 2012; Höning et al., 2014; Lackey et al., 2012; Samadi et al., 2014; Zhou et al., 2017). In general, the spessartine-rich garnet can be formed by direct crystallization from peraluminous magma in equilibrium with solid phases such as biotite and white mica at different temperature and

pressure conditions (Dahlquist et al., 2007). Depending on the temperature at which the spessartine-rich garnet was crystallizing, it could be of magmatic and/or metamorphic origin. It has been demonstrated that spessartine-rich garnet commonly crystallizes in equilibrium with S-type, aluminium- and manganese-rich granitic magma at relatively low pressures (Dahlquist et al., 2007; Zhang et al. 2012). However, du Bray (1988) claimed that manganese enrichment alone does not guarantee garnet nucleation and the presence of excess alumina in the magma may be a prerequisite for garnet nucleation. Therefore, the petrogenetic conditions and magmatic processes that control crystallization of spessartine-garnet in highly-fractionated granites are still controversial (Miller and Stoddard, 1981; Taylor and Stevens, 2010; Villaros et al., 2009; Zhang et al. 2012).

The Eastern Desert of Egypt, as a part of the Arabian-Nubian Shield, contains large volumes of Neoproterozoic granites (Fig. 1). The majority of the granites in the Eastern Desert of Egypt are garnet-free rocks. However, the spessartine-rich garnet has been recorded in some highly-fractionated rare metal granites and pegmatites from the Eastern Desert of Egypt (Abdalla et al., 1994;

* Corresponding author. E-mail: mabrouk.hassan@mu.edu.eg

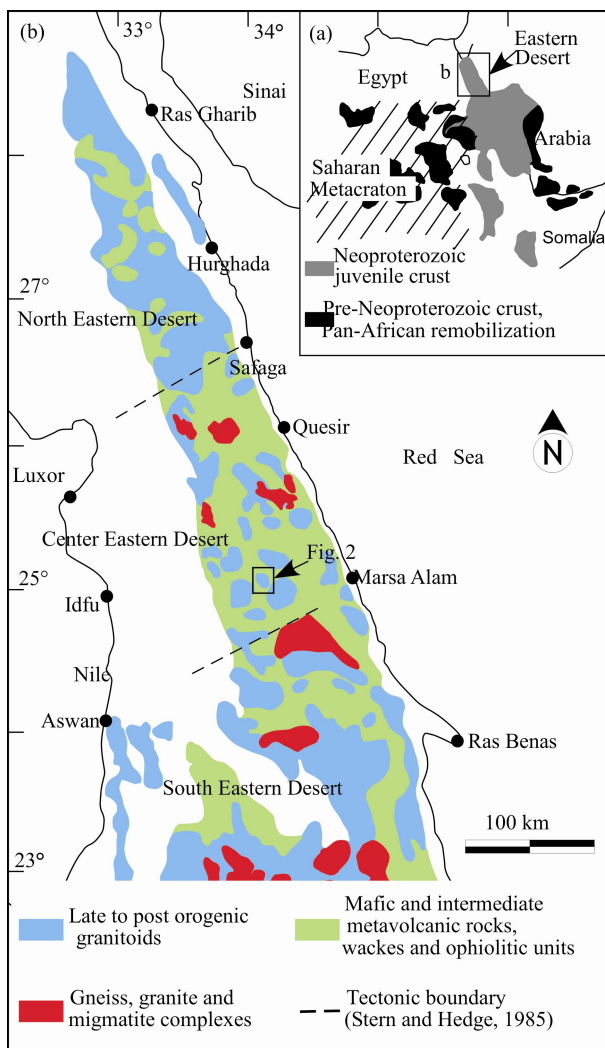


Fig. 1. (a) Schematic map of NE Africa showing the Arabian-Nubian Shield, the Saharan Metacraton, and Archaean and Palaeoproterozoic crust that was remobilized during the Neoproterozoic; (b) Geological map of the Eastern Desert of Egypt showing the location of the study area (modified after Ali et al., 2015; Stern and Hedge, 1985).

Helba et al., 1997). The Neoproterozoic (585 ± 24 Ma; Sami et al., 2018) Abu-Diab intrusion represents one of those highly-fractionated granites in the Central Eastern Desert of Egypt. Garnet is crystallized as an accessory mineral in the highly-evolved garnet-bearing muscovite granite at the margin of the Abu-Diab intrusion (Abu El-Ela et al., 2017; Sami et al., 2018). In this contribution, the textural features, zoning patterns, trace and REEs geochemistry of the garnet will be discussed with the objective of providing constraints on its origin in the host granite and its utility as a petrogenetic indicator and geochemical tracer.

2 Geological Settings

The Arabian-Nubian Shield continental crust (Fig. 1a) represents the northern segment of the East African Orogen. It was formed during the Neoproterozoic between

900 and 550 Ma through the accretion of intra-oceanic arcs, during the closure of the Mozambique Ocean and the amalgamation of Gondwana (Stern and Johnson, 2010). The Arabian-Nubian Shield consists of four main lithologies, including a juvenile island arc assemblage, ophiolites, gneisses and granitoid intrusions. The Neoproterozoic basement in the Eastern Desert of Egypt (Fig. 1b), comprises a dismembered ophiolite suite, island-arc metavolcano-sedimentary associations, arc metagabbro-diorite complex and I-type granitoids formed by microplate accretion related to subduction processes and collisional tectonics (720–630 Ma; Ali et al., 2012). During the post-orogenic stage (590–550 Ma), these rocks were intruded by large masses of mafic to felsic Dokhan volcanics and shallow level A-type granites (Eliwa et al., 2014). The Central Eastern Desert of Egypt is marked by two main tectonostratigraphic units: (1) the infrastructural unit (gneisses, migmatites, schists and amphibolites) and (2) Pan-African nappes including low grade metamorphosed ophiolite slices (serpentinites, pillow lavas and metagabbros), arc metavolcanics, and arc metasediments. These two units were intruded by syntectonic calc-alkaline granites and a metagabbro-diorite complex (606–614 Ma) and then by late to post-tectonic granites at ~ 590 –550 Ma (Farahat et al., 2011; Sami et al., 2017).

The Abu-Diab intrusion is considered to be one of the highest (~ 1160 m) mountainous granitic plutons in the Central Eastern Desert of Egypt. The Abu-Diab pluton occurs in the form of an oval-shaped body, covering approximately 20 km^2 between latitudes $25^\circ 12' \text{N}$ & $25^\circ 15' \text{N}$, and longitudes $34^\circ 11' \text{E}$ & $34^\circ 17' \text{E}$ (Fig. 2). The granites intruded into the surrounding metavolcanics, serpentinites, synorogenic calc-alkaline granodiorite, and metagabbro-diorite rocks at their eastern and northern sides with sharp and nonreactive contacts. The western and the southern parts of the pluton are surrounded by synorogenic calc-alkaline granitoid rocks (c. 655–570 Ma, El-Gaby et al. 1988) and pan-African ophiolitic serpentinites, but the contacts are hidden below wadi deposits.

The granites of the Abu-Diab pluton are massive, medium- to coarse-grained and become progressively fine-grained at the northern margin of the pluton. Based on field observations, colors, structural variations and petrographic investigations, the Abu-Diab massif constitutes a composite pluton consisting of three granitic phases. The two-mica (biotite and muscovite) granite constitutes the main phase and the large granitic mass in the core of the pluton. It is massive, medium- to coarse-grained with red-grey to reddish-pink colors. The margin of the pluton consists essentially of garnet-bearing muscovite granite and is cut by a small intrusion of muscovite granite at the north (Fig. 2). The garnet-bearing muscovite granite is medium-grained and shows variation in color from pink to red-colored blocks without significant changes in the petrographic and textural characteristics. Moreover, they are dissected by quartz veins and quartz fracture filling. Fluorites, in the form of veins, lenses and/or fissure filling, are scarcely encountered at the periphery of the pluton. No

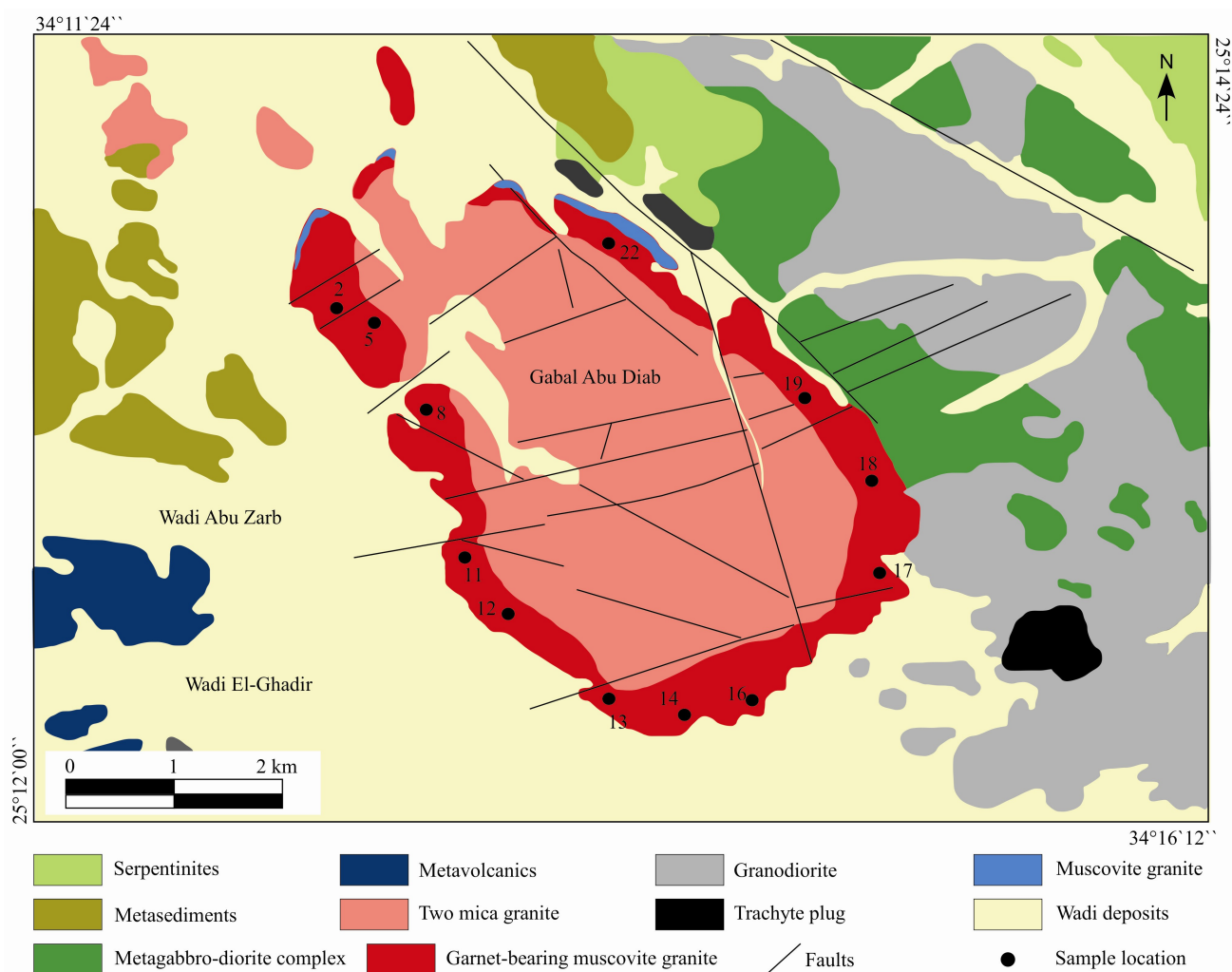


Fig. 2. Simplified geological map of the Abu-Diab intrusion showing the different lithological units in the area.

macroscopic planar, linear structural elements and/or xenoliths of metasedimentary rocks have been observed in the pluton (Abu El-Ela et al., 2017).

3 Petrography of the Abu-Diab Garnet-bearing Muscovite Granite

The garnet-bearing muscovite granite is relatively homogeneous, massive and reveals medium- to coarse-grained hypidiomorphic texture (Fig. 3a–c). The rock shows a mineral assemblage of plagioclase, quartz, K-feldspar, muscovite and garnet. In decreasing order of abundance, zircon, columbite, ilmenite, magnetite, rutile, ilmenorutile, chlorite, apatite, monazite and biotite are the minor and accessory phases. The K-feldspar phenocrysts and matrix are represented by orthoclase, microcline and perthitic microcline and sometimes show poikilitic texture in which plagioclase and quartz are enclosed. Plagioclase occurs as euhedral laths with well-developed polysynthetic twinning, but is free of oscillatory zoning (Fig. 3a–d). The K-feldspar is dominated by orthoclase (Or_{97-98}), while plagioclase (phenocrysts and matrix) is purely albite (An_0) with extremely low CaO content (Abu El-Ela et al.,

2017; Sami et al., 2018). Muscovite occurs as coarse-grained, euhedral to subhedral crystals of similar sizes to other rock-forming minerals (Fig. 3a–d). In a few cases, muscovite occurs as small fine lamellae which probably formed as replacement products of garnet (Fig. 3e). Biotite is rare and recorded as a minor mineral in a few thin sections. When present, it occurs as subhedral flakes, which sometimes enclose small albite and quartz crystals and/or intergrowth with muscovite.

4 Sampling and Analytical Methods

The fresh samples were systematically collected from the garnet-bearing muscovite granite at the margin of the Abu-Diab pluton. After detailed textural and petrographic studies, twelve polished sections of representative samples were selected for systematic major and trace element analysis of garnet. Garnet was investigated by transmitted light microscopy and back-scattered electron (BSE), prior to EMPA and LA-ICP-MS analysis.

Mineralogical analysis was conducted by using polished carbon-coated thin sections with a CAMECA SX100 electron microprobe equipped with four WDS and one

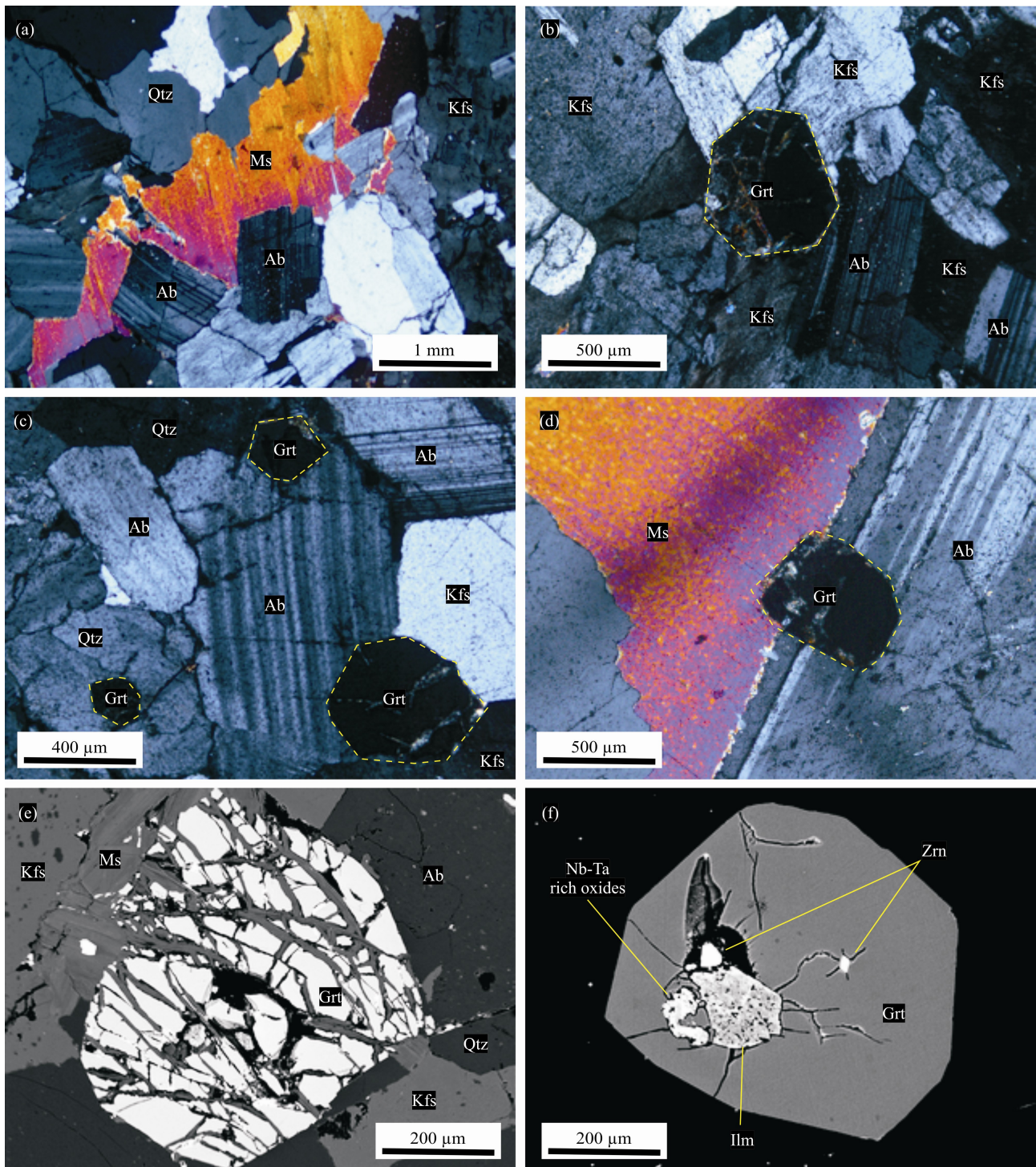


Fig. 3. Microphotographs (cross-polarized light) and BSE images showing the mineralogical and textural features of the Abu-Diab garnet-bearing muscovite granite.

(a) The general medium- to coarse-grains of muscovite, albite, K-feldspar and quartz reflecting the hypidiomorphic texture of the garnet-bearing muscovite granite; (b-d) Occurrence of euhedral to subhedral garnets with different grain size located in the interstices among quartz, albite and K-feldspar (b-c), or completely enclosed in magmatic quartz (c) and sharing boundaries between plagioclase and muscovite (d); (e-f) BSE images of subhedral cracked garnet crystal with some secondary muscovite replacing the garnet along the cracks (e) and hosting zircon, ilmenite, and Nb-Ta rich oxides (f). Mineral abbreviation: Qtz=quartz; Ab=albite; Kfs=k-feldspar; Ms=muscovite; Grt=garnet; Zrn=zircon; Ilm-ilmenite. All minerals labeled have been confirmed by EMPA.

EDS at the Department of Lithospheric Research, University of Vienna, Austria. All performed analyses were made against natural and synthetic mineral standards,

using four wavelength-dispersive spectrometers; acceleration voltage and beam current were 15 kV and 20 nA respectively. Natural and synthetic standards were

used for calibration, and the PAP correction (Pouchou and Pichoir, 1991) was applied to the data. A minimum of twelve analyses was obtained from each sample and four from each grain. X-ray compositional mapping was performed for selected elements in garnet using an energy-dispersive X-ray detector on the same equipment. The dwell time was set to 20 μ s at the highest possible resolution.

Trace elements and REEs of garnets were analyzed by LA-ICP-MS at the NAWI Graz Central Lab ‘Water, Minerals and Rocks’ (University of Graz and Graz University of Technology). The material was ablated by using a 193 nm laser pulsed at 10 Hz, 50 μ m spot size with an energy of ~ 7 J/cm². Helium was used as the carrier gas at ~ 0.7 l/min flow and data were acquired in time-resolved mode. For each analysis, a 30 second gas blank was obtained for background correction. LA-ICP-MS analyses were standardized using the NIST standard reference material (SRM) 610 of the National Institute of Standards and Technology, Gaithersburg, MD, USA. Values for the SRMs reported by Jochum et al. (2011) were applied for quantification of the results. The NIST SRM 612 standard was measured as an unknown to check for accuracy and reproducibility of the LA-ICP-MS analyses. Reproducibility of all REE elements for the standard measurements lies within a relative error of $<5\%$ for the NIST SRM 612 standard during each standard run. Time averaged concentration values of the LA-ICP-MS analyses were obtained using GLITTER (ver. 4.0) (Macquarie University, Sydney).

5 Results

5.1 Garnet petrography

Under the microscope, garnets are usually euhedral to subhedral and reddish-brown with variable grain sizes (50–500 μ m), composing less than one modal percent of the rock. It is often enclosed in quartz (Fig. 3c) and sometimes located in interstitial spaces between quartz, feldspars and muscovite (Fig. 3b–d). It appears to be in equilibrium with the other constituents due to the complete absence of any observable reaction rims between garnet and the other mineral constituents. Some garnet grains are partially replaced by and/or filled with secondary muscovite as a replacement product due to garnet alteration along fractures (Fig. 3e). Most of the small-sized garnets (≤ 100 μ m) are inclusion-free (Fig. 4a–b), while the large-sized (> 400 μ m) groundmass garnets are fractured and occasionally contain inclusions of quartz, zircon, Nb-Ti oxides and ilmenite, forming late during the crystallization of the leucocratic minerals (Figs. 3f and 4a–b). Detailed petrographic and electron microprobe studies show that the studied garnet is generally homogeneous (Fig. 4a) and, in rare cases, it shows weak zonation (Fig. 4b).

5.2 Mineral chemistry

5.2.1 Major element composition of garnet

The major element compositions and end-member formulae of the garnets are given in Table 1. Electron microprobe analyses show that garnets contain appreciable amounts of MnO (26–30 wt%), FeO (12–16 wt%), Al₂O₃

(19.8–20.5 wt%) and SiO₂ (35.3–36.3 wt%), with lesser amounts of MgO (0.35–0.94 wt%) and CaO (0.14–0.40 wt%), yielding an end-member formula of Sps_{61–72}Alm_{25–35}Prp_{1–4}Adr_{0–1}. The high MnO/(FeO + MnO) ratios of garnet (0.62–0.71) suggest that they are more evolved (Müller et al., 2012). It is important to note that all garnet crystals are of the spessartine-almandine solid solution, where the ratio of spessartine and almandine together exceeds 95 mol. %, identical to those recorded in highly-fractionated granites (Abdalla et al., 1994; Helba et al., 1997; Zhou et al., 2017).

No remarkable difference is recorded in the composition between the core and rim of the homogeneous garnet (Fig. 4a). In contrast, the zoned crystals show a slight difference in chemistry between the core and rim where the core is enriched in almandine and pyrope and depleted in spessartine and andradite relative to the rim (Fig. 4b). Moreover, the X-ray elemental map of zoned crystal (Fig. 5) exhibits the homogeneous distribution of Al and Nb, a slight difference in Fe and Mn and apparently significant changes in concentrations of both Ti and Mg between core and rim.

5.2.2 Trace and rare earth elements

The ore metal, trace and rare earth element compositions of garnet are given in Table 2. The garnets contain a very low concentration of Nb (≤ 3.46 ppm), Ta (≤ 0.97 ppm), W (≤ 0.40 ppm) and Cu (≤ 0.68 ppm). By comparison, it has higher and variable concentrations of Zn (195–356 ppm), Sn (22–138 ppm) and Li (67–92 ppm). In general, garnet is depleted in large ion lithophile elements (LILE) with lower values of Ba, Nb and Sr relative to the primitive mantle (Sun and McDonough, 1989) (Table 2, Fig. 6a). This is due to the larger ionic size of these elements, when compared to the size of the octahedral and eight coordination sites of the garnet structure (Gaspar et al., 2008).

The garnet contains high amounts of HREE (681–2494 ppm) and Y (1616–2827 ppm) and is depleted in LREE (3–11 ppm) and Eu (0.04–0.16 ppm) with both LREE/HREE and (La/Yb)_N ratios approaching zero. It is noted that the rims of the zoned garnet crystals contain much higher HREE and have relatively high Σ REE and low Σ LREE/ Σ HREE ratios, relative to the core (Table 2 and Fig. 6b). In general, the chondrite-normalized REE patterns of the studied garnet show HREE enrichment with significantly negative Eu anomalies.

5.3 Crystallization conditions

Garnets can be used as a potentially useful geothermometer due to slow diffusion rates of cations and anions and therefore zonation in garnets can record a substantial part of a rock's pressure-temperature history (Spear et al., 1984). Experimentally, as temperatures decrease, Mn can diffuse into garnet during Fe-Mn exchange with ilmenite (Pownceby et al., 1987). Therefore, the coexistence of garnet and ilmenite could provide a precise and accurate geothermometer relative to others, due to its accurate calibration, temperature sensitivity, as well as the chemical and structural simplicity of the crystalline solutions involved. As shown in Figure 4b, the

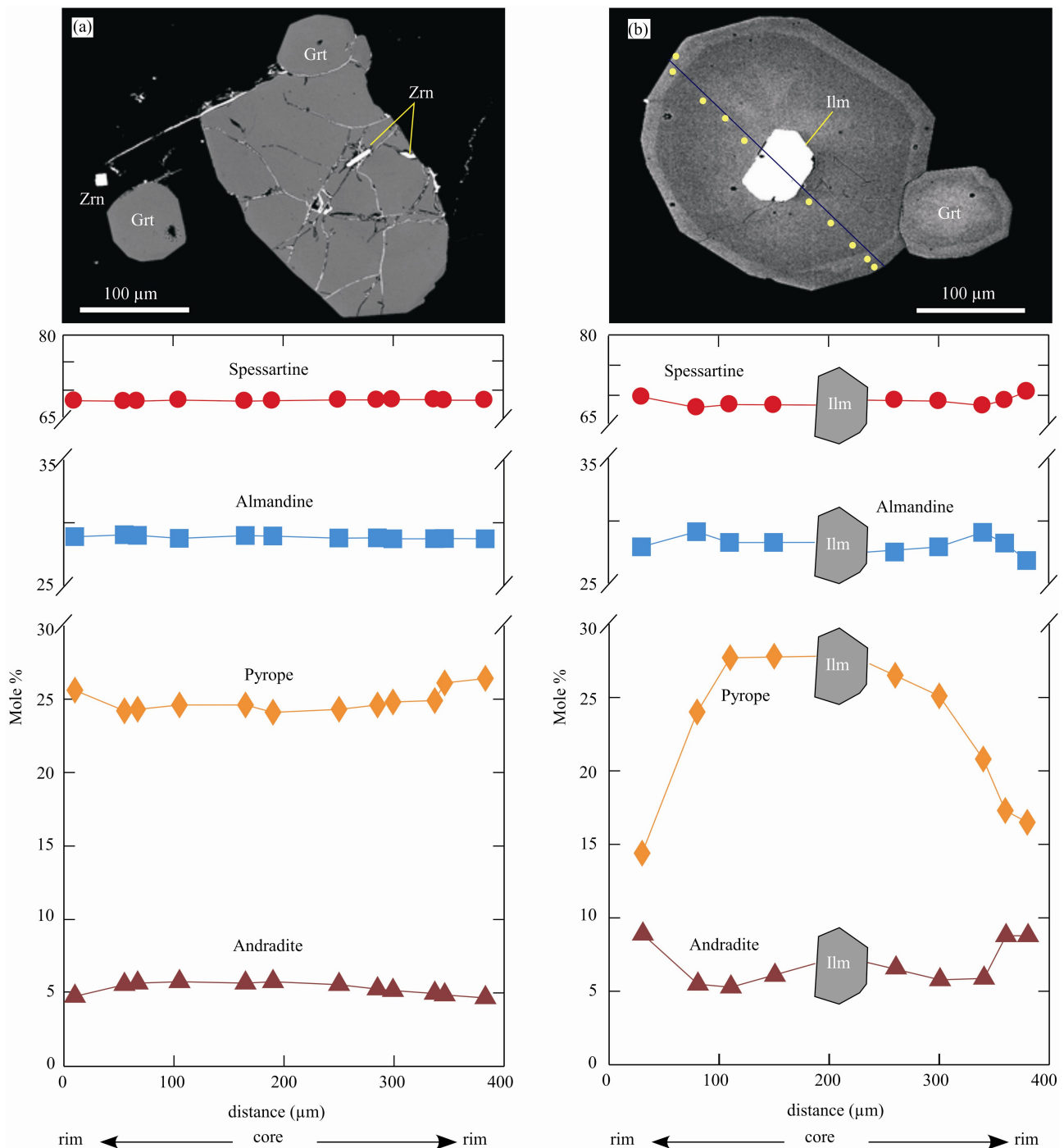


Fig. 4. (a) Variation in the end-members of representative homogeneous subhedral to euhedral garnet crystals that enclose small zircon crystals; (b) zoned euhedral garnet crystal host ilmenite from garnet-bearing muscovite granite (note that the small garnet crystal is free of inclusions). Solid circles and numbers represent analytical spots and their symbols.

idiomorphic garnet hosts a well-developed euhedral ilmenite crystal which has high Mn contents (up to 29 mol.% pyrophanite; Table 3). Accordingly, the calculated temperature of their formation ranges between 591°C and 646°C (Table 3).

Experimental studies have shown that almandine pyrope-enriched garnets are normal products of (early magmatic) medium-pressure crystallization of peraluminous magmas

(Clemens and Wall, 1981), while the progressive increase of Mn in the granitic liquid led to the crystallization of spessartine-rich garnet at relatively low pressures, estimated as low as 2 to 3 kbar by Speer and Becker (1992) and even as low as 1 kbar by Clemens and Wall (1981). The studied garnet is generally spessartine-almandine solid solution, which means that the host magma of the studied garnets was emplaced to shallower

Table 2 Representative trace and rare earth elements (ppm) of garnets from the Abu-Diab garnet-bearing muscovite granite, Central Eastern Desert of Egypt

Grains Texture	D5/1		D5/2	D5/3	D5/4	D5/5	D18/1		D18/2	D18/3		D18/4	D18/5	D18/6	D18/7	D5/6	
	core	rim	core	core	core	core	core	core	core	core	rim	core	core	core	core	core	rim
Li	72	92	76	72	73	73	83	86	79	87	68	67	71	73	68	82	83
Be	0.12	0.15	0.12	0.15	0.14	0.12	0.17	0.13	0.14	0.14	0.14	0.11	0.15	0.14	0.14	0.09	0.20
B	0.63	0.55	0.60	0.54	0.60	0.61	0.52	0.51	0.88	0.59	0.50	0.51	0.90	0.52	0.50	0.61	0.64
Ti	860	1319	890	895	943	934	718	617	1039	933	796	804	943	660	1177	686	775
V	4.7	7.2	6.6	6.6	6.5	6.7	6.3	3.8	4.6	4.9	6.1	5.4	4.8	13.3	5.9	13.1	14.1
Cr	1.9	2.0	2.1	2.4	1.9	1.9	2.0	1.9	1.9	2.0	2.0	2.0	2.1	2.0	2.0	2.0	2.4
Co	1.7	1.5	2.0	1.8	1.9	1.8	1.9	1.5	1.5	1.6	1.7	1.9	1.6	3.7	1.7	3.6	4.1
Ni	0.20	0.25	0.14	0.20	0.16	0.17	0.10	0.16	0.21	0.16	0.16	0.16	0.13	0.27	0.23	0.17	0.20
Cu	0.54	0.58	0.54	0.61	0.55	0.53	0.56	0.52	0.57	0.55	0.60	0.53	0.68	0.55	0.60	0.57	0.58
Zn	331	315	327	328	330	326	356	313	297	331	320	317	328	196	307	195	199
Ga	61	67	63	64	61	60	56	52	66	64	60	60	62	45	62	46	46
Rb	0.29	0.48	0.30	0.38	0.27	0.41	0.28	0.17	0.27	0.25	0.23	0.34	0.26	0.30	0.30	0.27	0.40
Sr	0.13	0.46	0.20	0.19	0.21	0.26	0.15	0.04	0.12	0.11	0.14	0.14	0.10	0.17	0.14	0.21	0.23
Y	1999	2827	2369	2348	2289	2308	2050	1616	2576	2387	2054	2058	2203	1693	2075	1675	2036
Zr	8.53	11.96	7.94	8.00	7.94	8.56	6.20	4.32	8.00	8.02	6.64	7.04	8.84	4.99	9.67	4.81	6.20
Nb	0.72	3.64	0.56	0.45	0.97	0.69	0.25	0.24	0.85	0.80	0.28	0.43	1.06	0.18	2.65	0.19	0.27
Sn	92	138	94	91	87	96	53	22	43	59	81	73	84	32	137	30	36
Cs	0.05	0.05	0.05	0.06	0.05	0.04	0.04	0.04	0.05	0.05	0.05	0.05	0.05	0.06	0.06	0.05	0.06
Ba	0.08	0.09	0.09	0.08	0.12	0.09	0.05	0.10	0.11	0.07	0.12	0.09	0.13	0.08	0.12	0.08	0.08
Hf	1.08	1.73	1.20	0.99	1.09	1.08	0.70	0.62	1.07	1.17	0.88	0.97	1.18	0.28	1.33	0.23	0.30
Ta	0.23	0.97	0.19	0.21	0.33	0.31	0.10	0.07	0.25	0.22	0.17	0.17	0.31	0.07	0.76	0.07	0.10
W	0.21	0.40	0.23	0.32	0.30	0.26	0.22	0.13	0.20	0.27	0.16	0.21	0.13	0.21	0.15	0.20	0.29
Tl	0.04	0.03	0.04	0.03	0.03	0.04	0.03	0.03	0.03	0.03	0.03	0.04	0.03	0.03	0.03	0.04	0.04
Pb	0.03	0.04	0.03	0.04	0.02	0.02	0.03	0.03	0.03	0.02	0.03	0.02	0.03	0.02	0.03	0.03	0.02
Th	0.02	0.01	0.01	0.01	0.01	0.01	0.01	0.01	0.01	0.01	0.01	0.01	0.01	0.01	0.01	0.01	0.01
U	0.18	0.32	0.17	0.14	0.18	0.17	0.09	0.08	0.25	0.18	0.11	0.12	0.22	0.08	0.24	0.07	0.09
La	0.01	0.01	0.01	0.01	0.01	0.01	0.01	0.01	0.01	0.01	0.01	0.01	0.02	0.01	0.01	0.01	0.01
Ce	0.01	0.01	0.01	0.01	0.01	0.01	0.01	0.01	0.01	0.01	0.01	0.01	0.01	0.01	0.02	0.02	0.01
Pr	0.02	0.02	0.01	0.01	0.02	0.01	0.01	0.01	0.01	0.01	0.01	0.01	0.02	0.01	0.03	0.01	0.01
Nd	0.43	0.78	0.47	0.49	0.41	0.50	0.32	0.19	0.40	0.48	0.31	0.38	0.46	0.13	0.65	0.20	0.26
Sm	8.54	10.14	7.61	7.61	7.06	7.50	5.67	6.28	7.89	8.40	6.15	7.09	8.54	2.60	10.30	2.82	3.68
Eu	0.06	0.06	0.05	0.06	0.07	0.05	0.04	0.08	0.07	0.07	0.06	0.07	0.06	0.15	0.06	0.16	0.13
Gd	57	57	55	52	52	49	47	58	72	65	48	52	63	30	58	28	35
Tb	30	31	31	31	29	28	28	32	42	37	28	30	35	17	30	17	20
Dy	306	343	329	325	318	309	290	288	415	363	301	307	341	213	289	211	256
Ho	66	95	79	81	79	80	71	47	86	80	74	71	73	63	60	59	81
Er	206	429	283	304	290	316	244	118	243	256	263	230	224	251	187	247	330
Tm	37	111	57	60	60	70	43	17	37	43	51	40	37	49	37	51	66
Yb	274	1224	474	513	527	659	349	107	246	324	414	302	261	417	290	438	585
Lu	31	204	61	69	75	94	44	13	28	40	56	34	28	65	32	73	92
ΣHREE	1007	2494	1368	1433	1430	1606	1116	681	1168	1209	1236	1066	1062	1105	983	1125	1465
ΣLREE	9	11	8	8	8	8	6	7	8	9	7	8	9	3	11	3	4

crustal levels, promoting its crystallization under declining temperature and pressure conditions. In summary, the studied garnets (Mn-rich spessartine-almandine solid solutions) were crystallized under relatively low temperature and pressure conditions (e.g., 646–591°C and < 3 kbar).

6 Discussion

6.1 Garnet zonation

Garnet can preserve chemical zoning below its closure temperature, due to slow diffusion rates for most cations and its resistance to alteration (Samadi et al., 2014). The studied garnet is distinguished by its poorly expressed zoning (Fig. 5) which is considered typical of liquidus garnet (Green, 1977). Some authors (e.g., du Bray, 1988; Macleod, 1992) have attributed zoning in garnet to fractional crystallization. Normal zoning in garnet (Fe-rich rim) is generally attributed to growth in a metamorphic environment during prograde conditions, while reverse zoning (Mn-rich rim) may indicate metamorphic growth

during retrograde conditions (i.e. falling temperatures and fractional crystallization) (Deer et al. 1992). Accordingly, the studied garnets are weakly zoned with Mn-rich rims, typical of reverse zoning (Fig. 5). The rimward andradite enrichment in the studied garnets could be attributed to the subsolidus breakdown of plagioclase and the incorporation of its calcium component in the garnet rims (Deer et al., 1992). The high field strength elements (HFSE, such as Zr, Nb, Ta, Hf, and U) in the studied garnets are distributed in a manner similar to the REE, being slightly enriched at the rim (Fig. 6). This weak zonation could be produced due to crystallization of garnet rims at much lower pressures during the ascension of the granitic melt.

6.2 Origin and nature of garnet in the host granite

The integration of textural and chemical features of garnet is the key to determine its origin. Petrographically, the studied garnet is of magmatic origin, as evidenced by its presence as individual euhedral fine- to medium-grained inclusions within a magmatic quartz, interstitial between the major mineral phases and a lack of

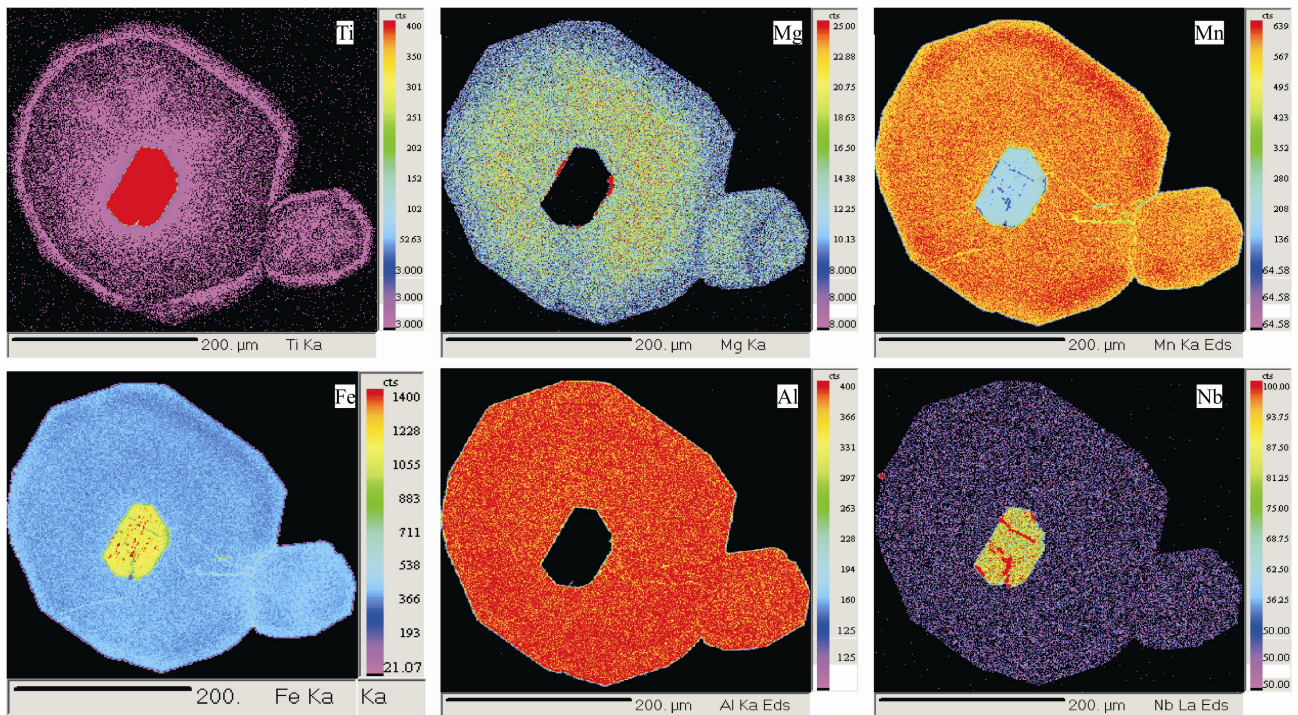


Fig. 5. Garnet X-ray composition maps showing a homogeneous distribution of Al, Fe, Nb, Mn and Mg, and variation in the distribution of both Ti and Mg between core and rim.

Table 3 EMPA data (wt%) used to calculate the thermometry of the studied garnet and ilmenite (cations on the basis of 12 and 3 oxygen for garnet and ilmenite, respectively)

Point	Grt-		Ilm-		Grt-		Ilm-	
	158	160	159	161	160	162	161	163
TiO ₂	0.28	47.07	0.25	50.32	0.27	50.17	0.27	49.67
Fe ₂ O ₃ ^a	0.60	9.19	0.61	4.13	0.51	3.91	0.46	4.47
FeO	12.90	28.41	12.70	31.79	12.67	31.87	12.83	31.20
MnO	28.87	13.47	28.89	12.96	29.03	12.74	28.98	13.00
MgO	0.67	0.02	0.63	0.01	0.66	0.03	0.68	0.02
Nb ₂ O ₅	–	0.87	–	1.14	–	1.17	–	1.04
ZnO	–	0.34	–	0.43	–	0.38	–	0.35
SiO ₂	35.98	0.04	36.18	0.04	35.98	0.03	36.09	0.02
Al ₂ O ₃	20.12	0.02	19.88	0.03	20.15	0.01	20.29	0.04
CaO	0.20	–	0.24	–	0.21	–	0.22	–
Total	99.6	99.4	99.4	100.9	99.5	100.3	99.8	99.8
Ti	0.02	0.905	0.02	0.952	0.02	0.954	0.02	0.949
Fe ⁺³	0.04	0.177	0.04	0.078	0.03	0.074	0.03	0.086
Fe ⁺²	0.89	0.607	0.88	0.669	0.88	0.674	0.88	0.663
Mn	2.02	0.291	2.03	0.276	2.04	0.273	2.02	0.280
Mg	0.08	0.001	0.08	0.000	0.08	0.001	0.08	0.001
Nb	–	0.011	–	0.015	–	0.015	–	0.014
Zn	–	0.006	–	0.008	–	0.007	–	0.007
Si	2.98	0.001	3.00	0.001	2.98	0.001	2.98	0.000
Al	1.96	0.001	1.94	0.001	1.97	0.000	1.97	0.001
Ca	0.02	–	0.02	–	0.02	–	0.02	–
Total	8.01	2.00	8.00	2.00	8.01	2.00	8.01	2.00
Sp	67.09		67.44		67.57		67.21	
Alm	29.59		29.27		29.11		29.37	
Py	2.73		2.57		2.69		2.76	
Andr	0.59		0.71		0.63		0.65	
Ilm		67.60		70.80		71.20		70.30
Prm		32.40		29.20		28.80		29.70
T°C ^b	658		599		591		608	

Note: ^aFe₂O₃ determined by stoichiometry, ^bTemperature were calculated using GPT excel spreadsheet (Reche et al., 1996).

replacement textures with other minerals (Fig. 3b–e). The small garnet crystals have no inclusions, while the coarser

ones contain randomly-oriented euhedral ilmenite and/or small euhedral zircons, identical in appearance to those included in other phenocryst minerals (Fig. 4a–b). Except for the zircon and ilmenite, garnet is clear and inclusion-free from typical metamorphic minerals. These textural features support the magmatic origin of garnet and enhance its formation by direct crystallization from the host magmas.

Several mechanisms were proposed for the origin of garnet, where it could occur as; (1) a restite phase during partial melting (René and Stelling, 2007); (2) xenocrysts derived from partially-assimilated metamorphic rocks (Erdmann et al., 2009); (3) peritectic garnet derived from wall rock or xenolith material that reacted with the host magma (Dorais and Tubrett, 2012; Taylor and Stevens, 2010); (4) secondary metasomatic garnet formed by the interaction between post-magmatic hydrothermal fluids and the hosting granites (Clarke and Rottura, 1994; Kontak and Corey, 1988); (5) phenocrysts which crystallized at high pressure ($P \geq 7$ kb) and survived transport to higher crustal levels (Harangi et al., 2001); and (6) crystals precipitated from differentiated Mn-enriched peraluminous magmas at low to moderate pressures (du Bray, 1988; Miller and Stoddard, 1981; Yang et al., 2013). The garnet in the Abu-Diab garnet-bearing muscovite granites is euhedral to subhedral, free of metamorphic mineral inclusions (Figs. 3 and 4) and contains extremely low concentrations of CaO (≤ 0.3 wt%) and high spessartine contents (MnO ≥ 26 wt%) (Table 1), quite distinct from garnet that was formed at high pressure and thus has relatively high CaO (> 5 wt%) and low MnO (< 2 wt%) contents (Harangi et al., 2001). These characteristics indicate these garnets do not have

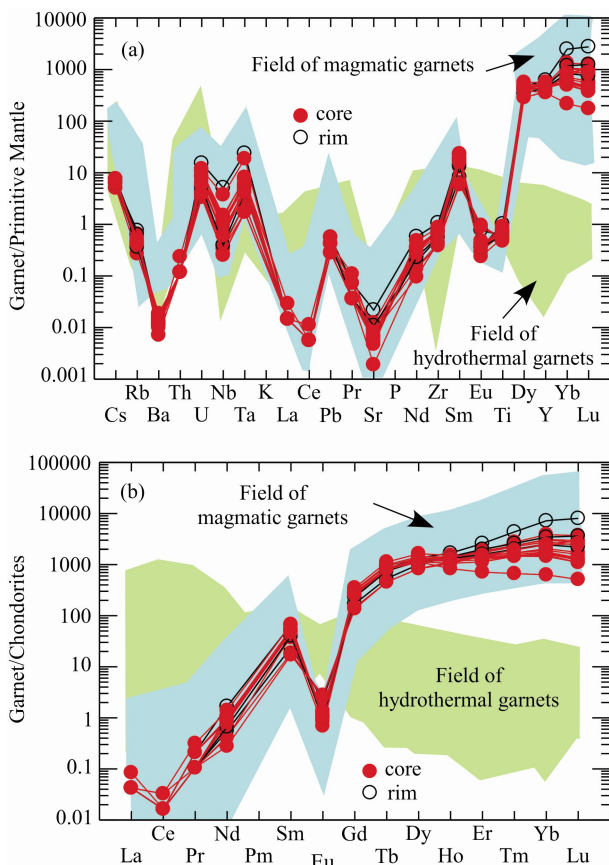


Fig. 6. (a) Primitive mantle normalized incompatible element spider diagram; (b) Chondrite-normalized REE patterns of the garnets from the Abu-Diab garnet-bearing muscovite granite. Fields of magmatic and hydrothermal garnets from Zhou et al. (2017) and references therein. Samples were normalized to chondrite and the primitive mantle values of Sun and McDonough (1989).

xenocrystic or restite origins and were not derived from wall rock metasediments. Moreover, the studied garnets have high spessartine molecule contents (61–72 mol. %) with low $Mg^{\#}$ values [$10^{\#}Mg / (Mg + Fe) = 0.47\text{--}1.12$; Table 1] which argue against the peritectic origin (Taylor and Stevens, 2010). The elevated HREE contents and significantly negative Eu anomalies of the analyzed garnets are similar to the REE compositions of other magmatic garnets and contrast sharply with hydrothermal garnets worldwide (Fig. 6b). Therefore, the studied spessartine-rich garnet in highly-fractionated garnet-bearing muscovite granite has a typical magmatic origin. This is further supported by the ternary discrimination diagram of Miller and Stoddard (1981), where all of the analyzed garnet crystals fall into the magmatic field (Fig. 7), suggesting a magmatic rather than hydrothermal origin of garnet. Also, using the trace and REE of the studied garnets in comparison with those obtained from magmatic and hydrothermal garnet from elsewhere around the world (Fig. 6a–b), it is clear that the garnets have similar REE patterns to magmatic garnets and completely different from those of hydrothermal origin worldwide (Zhou et al., 2017 and references therein). It is important to note that

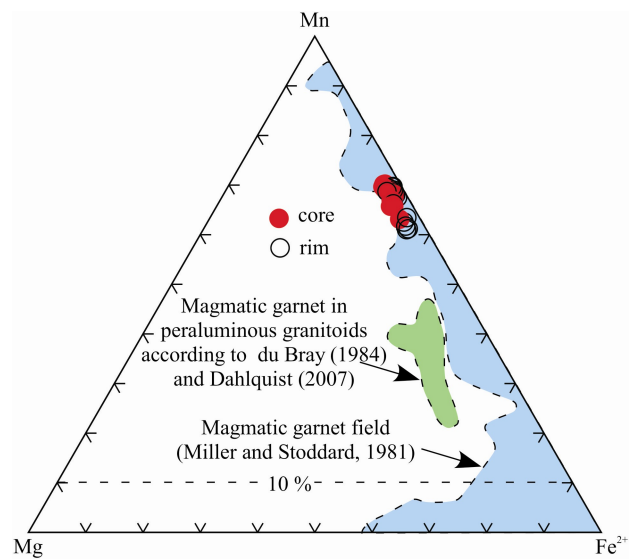


Fig. 7. Garnet compositions ($Mg\text{--}Mn\text{--}Fe^{2+}$) from the Abu-Diab garnet-bearing muscovite granite modified according to Dahlquist et al. (2007). The bluish field denotes the garnet compositions from the compilation of Miller and Stoddard (1981), and the garnet compositions in peraluminous granites are from du Bray (1988) and Dahlquist et al. (2007). The compilation of Miller and Stoddard (1981) revealed that an overwhelming majority of garnets found in granitoid contain > 10% spessartine component.

except for the partial transformation of garnet to chlorite and/or secondary muscovite along microcracks and interstitial fractures (Fig. 3b–e), the post-magmatic fluids have no significant effect on the structure and composition of the studied garnets.

6.3 Genesis of garnet

In general, magmas initially contain very little manganese. As such, it is to be expected that pure or almost pure spessartine garnet will crystallize due to the high concentration of Mn in the terminal stages of magma crystallization. Moreover, spessartine-rich garnet crystallizes when the liquid and muscovite become saturated with Mn^{2+} (Abbott, 1985). Since muscovite does not concentrate MnO relative to garnet, the crystallization and widespread occurrence of muscovites in the Abu-Diab garnet-bearing muscovite granite led to increasing MnO in the magma. Therefore, the appearance of garnet late during fractional crystallization is probably attributed to strong partitioning of Mn^{2+} in the liquid relative to muscovite. The homogeneity and absence of complex zoning in the studied spessartine garnets (Figs. 3 and 4), all indicate that the garnets grew from a compositionally homogeneous liquid, rich in Mn, in order to sustain garnet growth at low pressure and temperature.

Textural equilibrium of the studied garnets with other phases indicates that they could be crystallized directly from the melt in response to high MnO relative to $FeO + MgO$ and/or may have grown by reaction between earlier-formed biotite and silicate liquid. As for the other highly-fractionated peraluminous garnet-bearing granites

elsewhere (e.g., Miller and Stoddard, 1981), the possible reaction that controls garnet paragenesis in the Abu-Diab garnet-bearing muscovite granite is $\text{biotite} + \text{MnO} + \text{Al}_2\text{O}_3 + \text{SiO}_2$ (from liquid) = garnet+muscovite. This means that with increasing magma differentiation, spessartine-rich garnets will precipitate, followed by the disappearance of biotite. The exclusive occurrence of garnets and complete disappearance and/or very rare occurrence of biotite in garnet-bearing muscovite granite (Fig. 3a–d), supports the above mechanism and indicates that the studied spessartine garnet was formed at the expense of biotite in a highly-evolved MnO-rich magma.

The last scenario for the genesis of spessartine garnet in the Abu-Diab intrusion is that Mn - rich garnet could crystallize from Mn - rich fluids that exsolved from the fractionated silica-rich magma as suggested by Whitworth (1992) and Hildreth (1981). This model involves hydroxyl complexing of Mn in an ascending fluid phase to produce discrete areas of Mn enrichment in the roof zone of the magma chamber. Accordingly, the aqueous fluids released during the evolution of the Abu-Diab granitic melt are believed to have complexed the available Mn and transported it to the nucleation sites, allowing garnets to crystallize, while the chemistry of the melt as a whole evolved (Whitworth, 1992). This model may also explain the exclusive occurrence of spessartine garnet in the marginal granitic phase of the Abu-Diab intrusion.

6.4 Petrogenetic implications

The interpretation of garnet textures, chemistry, zonation and crystallization conditions will greatly help to define the magmatic and subsolidus crystallization histories of their host granites. The appearance of garnet late in the fractional crystallization of muscovite-saturated granitic magmas is probably due to the partitioning of manganese into the liquid rather than into early minerals.

The garnet-bearing granites are recorded in all petrogenetic types of granites, but the majority belong to S-type, which formed by partial melting of metasedimentary crustal rocks (Dahlquist et al., 2007; Taylor and Stevens, 2010). In a few cases, garnet-bearing granites could have I- and A-type magma characters with different origins in both anorogenic and extensional environments (du Bray, 1988; Hönig et al., 2014; Zhang et al., 2017). Some authors (e.g., Mohamed and Abu El-Ela, 2011; Shahin, 2015; Sami et al., 2018) have classified the Abu-Diab garnet muscovite granite as A-type granite due to their high $\text{FeO}^{\text{I}}/\text{MgO}$ ratios and extremely low MgO, CaO and V contents. However, Abu El-Ela et al. (2017) noted that the Abu-Diab granitic phases are not completely consistent with A-type granite, owing to their low high field strength element (HFSE) contents (e.g. REE, Zr, and Y). The chemical composition of garnet can give insights into the nature and type of the granitic magma of its host. Zhang et al. (2012 and references therein) used the reported major elements of magmatic garnets from various granites in the literature and the results are summarized in figure 8. The studied garnets are plotted within and at the boundary of the A-type granite field (Fig. 8), confirming their A-type granite affinity and reflecting the highly-fractionated nature of their host garnet-bearing muscovite

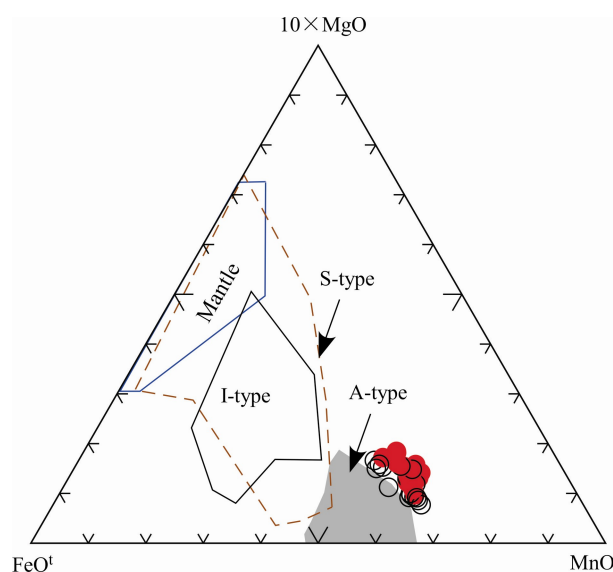


Fig. 8. FeO - $10\times\text{MgO}$ - MnO triangular diagram of garnet from various genetic granite types. Fields of garnets from I-, S- and A-type granites and igneous rocks originating from the mantle are from Zhang et al. (2012) and references therein.

granite.

It is possible from the garnet chemistry and from the relative proportion of various garnet end members, to know the possible origin of granitic magmas and also the approximate depth of formation (Whitworth, 1992). In general, almandine-rich garnets are associated with less well-evolved granitic rocks, possibly generated at greater depths than more evolved granites which contain high-spessartine garnets (du Bray, 1988). Therefore, the crystallization of high spessartine garnets within the Abu-Diab granites (Table 1; Fig. 4) confirms that they were formed at a shallower crustal depth (~ 15 km; Abu El-Ela et al., 2017) in highly-fractionated granitic magmas.

The temperature of formation for the reverse zoning idiomorphic garnet ranges between 591°C and 646°C (Table 3). These temperatures represent the minimum temperature of Abu-Diab garnet formation (i.e. garnet was crystallized later in the magma) when compared with the upper temperature limit of their host garnet-bearing muscovite granite, as inferred from zircon saturation temperatures ($733\pm 28^\circ\text{C}$; Abu El-Ela et al., 2017). The Abu-Diab garnet-bearing muscovite granite is rich in fluorine as indicated from both whole-rock ($\text{F} = 1735\text{--}2460$ ppm) and muscovite ($\text{F} = 2.08\text{--}2.83$ wt%) (Sami et al., 2018). Experimentally, fluorine can extend the eutectic temperature range of granite crystallization up to 560°C for fluorine-rich granite (Manning, 1981). As a consequence, the measured temperature indicates that the garnet in the host granite is crystallized later from the granitic magma and is formed as a result of the accumulation of the manganese element in the residual melt, because manganese is an incompatible element for the minerals (e.g. feldspar and muscovite) of granite.

Based on LA-ICP-MS analyses of garnets, the progressive increase of HREE from core to rim (Table 2;

Fig. 6) indicates that the rim was directly crystallized from the relatively HREE-rich fluid. In general, the presence of HREE-enriched rims in garnet crystals can be attributed to the formation of minerals that fractionate LREE from HREE (e.g., monazite). The F-rich fluids have the capacity to transport immobile HFSE and HREE elements (Agangi et al. 2010). Therefore, during the late magmatic stage of the Abu-Diab garnet-bearing muscovite granite, fluorine dissolved in the magma is concentrated in the fluids, causing REE and HFSE complexing and mobilization (i.e. they behave as incompatible elements). The interaction of these fluids with the hot, solid granite led to the crystallization of spessartine garnet in the interstices between the major mineral phases of the Abu-Diab garnet-bearing muscovite granite.

7 Conclusions

(1) The garnet-bearing muscovite granite represents the highly-fractionated granitic body in the outer rim of the Abu-Diab intrusion, which is located in the Central Eastern Desert of Egypt (north Arabian-Nubian Shield). It consists of quartz, k-feldspars, albite and Li-phengite as major phases. The most important accessory minerals include garnet, columbite, zircon, rutile, ilmenorutile, ilmenite, apatite and monazite.

(2) Homogeneous to weakly-zoned garnet crystals are euhedral to subhedral and reddish-brown with variable grain size, enclosed in magmatic quartz and located in interstitial spaces between quartz, feldspars and muscovite. All studied garnet crystals have a spessartine-almandine solid solution and contain appreciable amounts of MnO, FeO, Al₂O₃ and SiO₂, with lesser amounts of MgO and CaO, yielding an end-member formula of Sps₆₁₋₇₂Alm₂₅₋₃₅Prp₁₋₄Adr₀₋₁. Moreover, the garnets contain a very low concentration of Nb, Ta, W and Cu, but contain higher and variable concentrations of Zn, Sn, Li Y and high \sum REE concentrations (especially HREE). The studied garnet was crystallized under relatively low temperature and pressure conditions (646–591°C and < 3 kbar) at shallower crustal levels.

(3) The chemistry and textural criteria of the studied garnet suggest a pure magmatic origin and support its formation by direct crystallization from the host magmas. The spessartine-rich garnet of the Abu-Diab garnet-bearing muscovite granite could be formed by hydroxyl complexing of manganese at the roof of the magma chamber and/or at the expense of biotite, and grew from compositionally homogeneous liquid rich in Mn in order to sustain garnet growth at low pressure and temperature.

(4) The chemistry of garnet confirms the A-type granitic affinity of the host, the highly-fractionated garnet-bearing muscovite granite. Fluorine-rich fluids play an important role during the formation of spessartine garnet in the Abu-Diab intrusion. These F-rich fluids have the ability to complex and mobilize the REE and HFSE and can extend the eutectic temperature of granite crystallization up to 560°C. During the late magmatic stage, the interaction of these F-rich fluids with the hot, solid granite led to the crystallization of HREE-rich minerals including spessartine garnet in the interstices between the major

mineral phases of the Abu-Diab garnet-bearing muscovite granite.

Acknowledgments

We thank Franz Kiraly for assistance with the electron microprobe and the staff and technicians of the Department of Lithospheric Research, University of Vienna, Austria. Thanks to the International Association of GeoChemistry (IAGC) for their grant (2017) to perform the geochemical analyses. We thank Prof. Dr. Mohammed Z. El-Bialy, an anonymous reviewer and the Editor-in-Chief Prof. Dr. Degan Shu for their constructive comments and suggestions; these led to a significant improvement of the manuscript.

Manuscript received Nov. 17, 2018

accepted Jan. 29, 2019

associate EIC: HAO Ziguo

edited by Jeff LISTON and FEI Hongcai

References

- Abbott, R.N., 1985. Muscovite-bearing granites in the AFM liquidus projection. *Canadian Mineralogist*, 23: 553–561.
- Abdalla, H., Matsueda, H., Ishihara, S., and Miura, H., 1994. Mineral chemistry of albite-enriched granitoids at Um Ara, Southeastern Desert, Egypt. *International Geology Review*, 36: 1067–1077.
- Abu El-Ela, F.F., Abu El-Rus, M.A., Mohamed, M.A., and Gahlan, H.A., 2017. Cold plutonism in the Arabian–Nubian Shield: evidence from the Abu Diab garnet-bearing leucogranite, central Eastern Desert, Egypt. *Journal of the Geological Society*, 174: 1031–1047.
- Agangi, A., Kamenetsky, V.S., and McPhie, J., 2010. The role of fluorine in the concentration and transport of lithophile trace elements in felsic magmas: Insights from the Gawler Range volcanics, South Australia. *Chemical Geology*, 273: 314–325.
- Ali, K.A., Kroner, A., Hegner, E., Wong, J., Li, S.Q., Gahlan, H.A., and Abu El Ela, F.F., 2015. U-Pb zircon geochronology and Hf-Nd isotopic systematics of Wadi Beitan granitoid gneisses, South Eastern Desert, Egypt. *Gondwana Research*, 27: 811–824.
- Ali, K.A., Moghazi, A.K.M., Maurice, A.E., Omar, S.A., Wang, Q., Wilde, S.A., Moussa, E.M., Manton, W.I., and Stern, R.J., 2012. Composition, age, and origin of the similar to 620 Ma Humr Akarim and Humrat Mukbid A-type granites: no evidence for pre-Neoproterozoic basement in the Eastern Desert, Egypt. *International Journal of Earth Sciences*, 101: 1705–1722.
- Clarke, D.B., and Rottura, A., 1994. Garnet-forming and garnet-eliminating reactions in a quartz diorite intrusion at Capovaticano, Calabria, Southern Italy. *Canadian Mineralogist*, 32: 623–635.
- Clemens, J.D., and Wall, V.J., 1981. Origin and crystallization of some peraluminous (S-type) granitic magmas. *The Canadian Mineralogist*, 19(1): 111–131.
- Dahlquist, J.A., Galindo, C., Pankhurst, R.J., Rapela, C.W., Alasino, P.H., Saavedra, J., and Fanning, C.M., 2007. Magmatic evolution of the Peñón Rosado granite: Petrogenesis of garnet-bearing granitoids. *Lithos*, 95: 177–207.
- Deer, W.A., Howie, R.A., and Zussman, J., 1992. *An Introduction to the Rock Forming Minerals*, Second Longman ed. Longman, London, 696.
- Dorais, M.J., and Tubrett, M., 2012. Detecting peritectic garnet in the peraluminous Cardigan Pluton, New Hampshire. *Journal of Petrology*, 53: 299–324.
- du Bray, E.A., 1988. Garnet compositions and their use as indicators of peraluminous granitoid petrogenesis-southeastern Arabian Shield. *Contributions to Mineralogy and*

- Petrology, 100: 205–212.
- El-Gaby, S., List, F.K., and Tehrani, R., 1988. Geology, evolution and metallogenesis of the Pan-African belt in Egypt. In: El-Gaby, S., and Greiling, R.O. (eds), *The Pan-African Belt of NE Africa and Adjacent Area*. Springer, Heidelberg, 17–68.
- Eliwa, H.A., Breitzkreuz, C., Murata, M., Khalaf, I.M., Bulhler, B., Itaya, T., Takahashi, T., Hirahara, Y., Miyazaki, T., Kimura, J.I., Shibata, T., Koshi, Y., Kato, Y., Ozawa, H., Daas, M.A., and El Gameel, K., 2014. SIMS zircon U-Pb and mica K-Ar geochronology, and Sr-Nd isotope geochemistry of Neoproterozoic granitoids and their bearing on the evolution of the north Eastern Desert, Egypt. *Gondwana Research*, 25: 1570–1598.
- Erdmann, S., Jamieson, R.A., and MacDonald, M.A., 2009. Evaluating the origin of garnet, cordierite, and biotite in granitic rocks: a case study from the South Mountain Batholith, Nova Scotia. *Journal of Petrology*, 50: 1477–1503.
- Farahat, E.S., Zaki, R., Hauzenberger, C., and Sami, M., 2011. Neoproterozoic calc-alkaline peraluminous granitoids of the Delehimmi pluton, Central Eastern Desert, Egypt: implications for transition from late- to post-collisional tectonomagmatic evolution in the northern Arabian-Nubian Shield. *Geological Journal*, 46: 544–560.
- Gaspar, M., Knaack, C., Meinert, L.D., and Moretti, R., 2008. REE in skarn systems: a LA-ICP-MS study of garnets from the Crown Jewel gold deposit. *Geochimica et Cosmochimica Acta*, 72: 185–205.
- Gharib, M.E., 2012. Origin and evolution history of magmatic garnet-bearing pegmatites and associated granitoids, Abu Had area, south Eastern Desert, Egypt: inference from petrology and geochemistry. *Journal of American science*, 8: 536–554.
- Green, T.H., 1977. Garnet in Silicic Liquids and Its Possible Use as a P-T Indicator. *Contributions to Mineralogy and Petrology*, 65: 59–67.
- Harangi, S., Downes, H., Kosa, L., Szabo, C., Thirlwall, M.F., Mason, P.R.D., and Matthey, D., 2001. Almandine garnet in calc-alkaline volcanic rocks of the northern Pannonian Basin (eastern-central Europe): Geochemistry, petrogenesis and geodynamic implications. *Journal of Petrology*, 42: 1813–1843.
- Helba, H., Trumbull, R.B., Morteani, G., Khalil, S.O., and Arslan, A., 1997. Geochemical and petrographic studies of Ta mineralization in the Nuweibi albite granite complex, Eastern Desert, Egypt. *Mineralium Deposita*, 32: 164–179.
- Hildreth, W., 1981. Gradients in silicic magma chambers: Implications for lithospheric magmatism. *Journal of Geophysical Research*, 86: 10153–10192.
- Hönig, S., Čopjaková, R., Škoda, R., Novák, M., Dolejš, D., Leichmann, J., and Galiová Michaela, V., 2014. Garnet as a major carrier of the Y and REE in the granitic rocks: An example from the layered anorogenic granite in the Brno Batholith, Czech Republic. *American Mineralogist*, 99: 1922.
- Jochum, K.P., Weis, U., Stoll, B., Kuzmin, D., Yang, Q.C., Raczek, I., Jacob, D.E., Stracke, A., Birbaum, K., Frick, D.A., Gunther, D., and Enzweiler, J., 2011. Determination of reference values for NIST SRM 610-617 glasses following ISO guidelines. *Geostandards and Geoanalytical Research*, 35: 397–429.
- Kontak, D.J., and Corey, M., 1988. Metasomatic origin of spessartine-rich garnet in the South Mountain Batholith, Nova Scotia. *Canadian Mineralogist*, 26: 315–334.
- Lackey, J.S., Romero, G.A., Bouvier, A.S., and Valley, J.W., 2012. Dynamic growth of garnet in granitic magmas. *Geology*, 40: 171–174.
- Macleod, G., 1992. Zoned manganese-rich garnets of magmatic origin from the Southern Uplands of Scotland. *Mineralogical Magazine*, 56(382): 115–116.
- Manning, D., 1981. The effect of fluorine on liquidus phase relationships in the system Qz-Ab-Or with excess water at 1 kb. *Contributions to Mineralogy and Petrology*, 76(2): 206–215.
- Miller, C.F., and Stoddard, E.F., 1981. The Role of Manganese in the paragenesis of magmatic garnet - an example from the old woman Piute Range, California - a reply. *Journal of Geology*, 89: 770–772.
- Mohamed, M.A., and Abu El-Ela, F.F., 2011. Geochemistry and fluid inclusions study of highly fractionated garnet-bearing granite of Gabal Abu Diab, central Eastern Desert of Egypt. *Arabian Journal of Geosciences*, 4: 763–773.
- Müller, A., Kearsley, A., Spratt, J., and Seltnann, R., 2012. Petrogenetic implications of magmatic garnet in granitic pegmatites from Southern Norway. *Canadian Mineralogist*, 50: 1095–1115.
- Pouchou, J.-L., and Pichoir, F., 1991. Quantitative analysis of homogeneous or stratified microvolumes applying the model “PAP”. In: Heinrich, K.F.J., and Newbury, D.E. (eds.), *Electron Probe Quantitation*. Springer US, Boston, MA, 31–75.
- Pownceby, M.I., Wall, V.J., and O'Neill, H.S., 1987. Fe-Mn partitioning between garnet and ilmenite - experimental calibration and applications. *Contributions to Mineralogy and Petrology*, 97: 116–126.
- Reche, J., and Martinez, F. J., 1996. GPT: An excel spreadsheet for thermobarometric calculations in metapelitic rocks. *Computers & Geosciences*, 22 (7): 775–784.
- René, M., and Stelling, J., 2007. Garnet-bearing granite from the Třebíč pluton, Bohemian Massif (Czech Republic). *Mineralogy and Petrology*, 91: 55–69.
- Samadi, R., Miller, N.R., Mirnejad, H., Harris, C., Kawabata, H., and Shirdashtzadeh, N., 2014. Origin of garnet in aplite and pegmatite from KhajehMorad in northeastern Iran: A major, trace element, and oxygen isotope approach. *Lithos*, 208: 378–392.
- Sami, M., Ntaflos, T., Farahat, E.S., Mohamed, H.A., Ahmed, A.F., and Hauzenberger, C., 2017. Mineralogical, geochemical and Sr-Nd isotopes characteristics of fluorite-bearing granites in the Northern Arabian-Nubian Shield, Egypt: Constraints on petrogenesis and evolution of their associated rare metal mineralization. *Ore Geology Reviews*, 88: 1–22.
- Sami, M., Ntaflos, T., Farahat, E.S., Mohamed, H.A., Hauzenberger, C., and Ahmed, A.F., 2018. Petrogenesis and geodynamic implications of Ediacaran highly fractionated A-type granitoids in the north Arabian-Nubian Shield (Egypt): Constraints from whole-rock geochemistry and Sr-Nd isotopes. *Lithos*, 304–307: 329–346.
- Shahin, H.A.E.A., 2015. Radioactivity, geochemical characteristics, and genetic relation of some younger granite plutons: example from central Eastern Desert, Egypt. *Arabian Journal of Geosciences*, 8: 7961–7972.
- Spear, F.S., Selverstone, J., Hickmott, D., Crowley, P., and Hodges, K.V., 1984. P-T Paths from garnet zoning - a new technique for deciphering tectonic processes in crystalline terranes. *Geology*, 12: 87–90.
- Speer, J.A., and Becker, S.W., 1992. Evolution of magmatic and subsolidus AFM mineral assemblages in granitoid rocks e biotite, muscovite, and garnet in the Cuffytown Creek, pluton, South-Carolina. *American Mineralogist*, 77: 821–833.
- Stern, R.J., and Hedge, C.E., 1985. Geochronologic and isotopic constraints on late Precambrian crustal evolution in the Eastern Desert of Egypt. *American Journal of Science*, 285(2): 97–127.
- Stern, R.J., and Johnson, P., 2010. Continental lithosphere of the Arabian Plate: A geologic, petrologic, and geophysical synthesis. *Earth-Science Reviews*, 101: 29–67.
- Sun, S.S., and McDonough, W.F., 1989. Chemical and isotopic systematics of oceanic basalts: implications for mantle composition and processes. *Geological Society, London, Special Publications*, 42: 313–345.
- Taylor, J., and Stevens, G., 2010. Selective entrainment of peritectic garnet into S-type granitic magmas Evidence from Archaean mid-crustal anatectites. *Lithos*, 120: 277–292.
- Villaros, A., Stevens, G., and Buick, I.S., 2009. Tracking S-type granite from source to emplacement: Clues from garnet in the Cape Granite Suite. *Lithos*, 112: 217–235.
- Whitworth, M. P., 1992. Petrogenetic implications of garnets associated with lithium pegmatites from SE Ireland. *Mineralogical Magazine*, 56(382): 75–83.
- Wu, F.Y., Sun, D.Y., Jahn, B.M., and Wilde, S., 2004. A Jurassic garnet-bearing granitic pluton from NE China showing tetrad

- REE patterns. *Journal of Asian Earth Sciences*, 23: 731–744.
- Yang, J.H., Peng, J.T., Hu, R.Z., Bi, X.W., Zhao, J.H., Fu, Y.Z., and Shen, N.P., 2013. Garnet geochemistry of tungsten-mineralized Xihuashan granites in South China. *Lithos*, 177: 79–90.
- Zhang, J.Y., Ma, C.Q., and She, Z.B., 2012. An Early Cretaceous garnet-bearing metaluminous A-type granite intrusion in the East Qinling Orogen, central China: Petrological, mineralogical and geochemical constraints. *Geoscience Frontiers*, 3: 635–646.
- Zhang, Y., Shao, Y.J., Wu, C.D., and Chen, H.Y., 2017. LA-ICP-MS trace element geochemistry of garnets: Constraints on hydrothermal fluid evolution and genesis of the Xinqiao Cu-S-Fe-Au deposit, eastern China. *Ore Geology Reviews*, 86: 426–439.
- Zhou, J.H., Feng, C.Y., and Li, D.X., 2017. Geochemistry of the garnets in the Baiganhu W-Sn ore field, NW China. *Ore Geology Reviews*, 82: 70–92.

About the first author and the corresponding author



Mabrouk SAMI was born in Abu-Hammad City, Sharkia Governate, Egypt. He is currently working as a senior lecturer of mineralogy and geochemistry at the Geology Department, Faculty of Science, Minia University, Egypt. He has completed his Ph.D. from the Department of Lithospheric Research, University of Vienna, Austria. He majors in geology and his field of study is the mineralogy, petrology, geochemistry and geochronology of crystalline rocks, and he has published several papers that concentrated on the petrogenesis and source of highly-fractionated granites and their related rare metal (Nb-Ta-Sn-W-Th-U-REE oxides) mineralization. Dr. Mabrouk Sami is a member of several international geological societies and unions. E-mail: mabrouk.hassan@mu.edu.eg; Phone: 002-01012008936.